Available online at www.sciencedirect.com

ScienceDirect

Proceedings of the Combustion Institute 36 (2017) 4391–4398

Proceedings of the Combustion Institute

www.elsevier.com/locate/proci

Thermal structure of methane hydrate fueled flames

F.H. Wu [a,*], R.E. Padilla [b], D. Dunn-Rankin [b], G.B. Chen [c], Y.C. Chao [a]

[a] Department of Aeronautics and Astronautics, National Cheng Kung University, Tainan 701, Taiwan, R.O.C.
[b] Deparment of Mechanical and Aerospace Engineering, 4200 Engineering Gateway, Irvine, CA, USA
[c] Research Center for Energy Technology and Strategy, National Cheng Kung, University, Tainan 701, Taiwan, R.O.C.

Received 4 December 2015; accepted 1 June 2016
Available online 17 June 2016

Abstract

An experimental and computational study investigates the burning behavior of methane hydrate in an opposed-jet porous burner. The free (convection) burning of methane hydrates is unstable and flame extinction can occur due to water film layer buildup or self-preservation phenomena. The burner allows us to overcome these problems and generates, for a limited time, a stable 1-D methane hydrate diffusion flame. Axial temperature, flame location, and flame width were measured using color-ratio thin filament pyrometry (TFP) from the radiative emission of a silicon carbide fiber that is oriented across the flame. The hydrate flame temperatures are found to be close to 1700 K. Computationally, chemical kinetic calculations with water vapor introduced into the fuel stream, and the opposed flame model and the GRI MECH 3.0 mechanism, simulated conditions of methane hydrate diffusion flames in order to observe the temperature, flame position and thermal width. The computational and experimental results showed close agreement in temperature and indicate that water from the hydrate dilutes the fuel and reduces flame temperatures to approximately 1700 K. TFP allowed us to capture the dynamic movement of the hydrate flame toward the air side as it burned robustly during a process where heat and mass transfer promoted a release in methane and water vapor entrainment into the reaction zone.

Keywords: Methane hydrate; Opposed-jet porous burner; Color-ratio pyrometry

1. Introduction

There is a major energy resource of methane hydrates found in earth's permafrost regions and seafloor [1]. Clathrate hydrates, also widely known as gas hydrates are ice-like crystalline solids composed of a network of hydrogen-bonded water molecules that form cages around a guest molecule [1]. Gas hydrates are nonstoichiometric compounds and are stable at elevated pressures and low temperatures. The geometry of the cages is a direct function of the guest molecule diameter, which ranges between 4 Å and 7 Å for structures, sI, sII, and sH hydrates. The structure sI is the most common for methane. Burning methane hydrates involve a combustion process where a large amount of water (H_2O) is naturally incorporated into the

* Corresponding author. Tel.: +886 6 2345291; fax: +886 6 238 9940.
E-mail address: bluehusky759@gmail.com (F.H. Wu).

http://dx.doi.org/10.1016/j.proci.2016.06.012
1540-7489 © 2016 by The Combustion Institute. Published by Elsevier Inc.

fuel stream since hydrates consist of 86% water and 14% methane by mole fraction and have a composition generally approximated as $CH_4 \bullet 5.75H_2O(s)$.

Methane hydrate combustion has not been studied extensively partially due to the complex multiphase change characteristic and partly due to the difficulty in working with a fuel that decomposes under standard temperature and pressure conditions. Some aspects include dissociation of methane hydrate CH_4 (gas) + H_2O (solid or liquid), that is, methane/air diffusive combustion, liquid water formation, vaporization of water, and ice formation. However, the direct combustion of methane hydrates generally suffers from unsteady flame behaviors and water dripping that leads to extinguishment [2]. During the direct methane mass release or direct combustion process of subcooled hydrate at atmospheric pressure, Istomin and Yakushev [3] found that a layer of water or ice is formed on the surface of methane hydrate, causing reduction of surface porosity and thus blocking the further release of methane. This phenomenon was recognized as "self-preservation" by Misyura and Nakoryakov [4]. The low temperature at which self-preservation exists (below 0 °C) and stability at these temperatures in atmospheric pressure has made hydrates an attractive topic for researchers as a method for transporting and storing natural gas instead of using liquefied natural gas (LNG) [5]. The rate of dissociation, nucleation and formation of hydrates depends on the solubility of gas in water, porosity, pressure, temperature, and the gas and salt concentration found in water solution [6]. Stern et al. [7] reported that the hydrate dissociation rate increases monotonically with temperature. Recently, more in depth studies of methane hydrate combustion have been undertaken. Kohany and Sirignano [8] proposed a revised model by including an intermediate layer of bubbly mixture to describe methane hydrate combustion and by assuming particles of initial radius of 100 μm or less to simplify the self-preservation effect. A theoretical model to identify the mass release process with self-preservation phenomenon is complicated and currently unavailable. Yoshioka et al. [2] studied the combustion behavior of a methane hydrate sphere under atmospheric pressure. In the combustion process, there are bubbles and water droplets formed on the hydrate surface leading to flame extinction. In addition, there are few experimental and numerical publications on flame spreading over pure methane hydrate in a laminar boundary layer ([9–11]) and methane hydrate spheres under normal gravity [2]. Taborek and Dunn-Rankin [12] proposed the concept of direct energy conversion by in situ combustion of methane hydrates and carbon dioxide sequestration in the deep ocean.

A novel cylindrical porous burner was proposed by Wu and Chao [13] to relieve the water film and self-preservation problem. The proposed burner can effectively use methane hydrate and sustain a stable flame during the burning process. Using such a burner, and presuming a counterflow configuration, theoretically, methane hydrate combustion can be categorized as a methane diffusion flame with a large amount of water vapor addition in the fuel stream. To approximate this behavior, Lee et al. [14] simulated the opposed jet combustion characteristics of nonpremixed water-laden methane flames. They found that the maximum flame temperature decreases with water addition and that flames can sustain water beyond molar ratios (H_2O/CH_4) of 4. The extinction limits are expanded with decreasing strain rates, meaning that more water vapor can be added for low strain rates. Consequently, in order to extract the key burning characteristics of methane hydrates, and in order to come closer to the opposed flow simulation, we use the geometrically simplified and more stable nonpremixed opposed jet porous burner. In order to study the thermal and chemical combustion characteristics of methane hydrate flames experimental results are compared with computations using the opposed flame model (i.e., counterflow diffusion flame configuration) to simulate methane hydrate combustion and to study the flame structure and extinction limit as a function of water addition to the methane fuel.

2. Methodology: experimental measurements and computational

2.1. Production of methane hydrate

The hydrates are made following the seeding method proposed by Stern et al. [15,16]. The procedure of the seeded material is made from ice which can provide higher methane content and shorter time to produce. The experimental configuration involves two vessels. One is for the reservoir and the other for a reaction. The pressure vessel is placed in a freezer to cool and initially hold temperature and pressure below 260 K and 1500 bar. The reaction vessel is used to pressurize CH_4 (high purity > 99.999 %) gas and hold the molds that are used for making the hydrate samples. The molds consist of a hollow split cylinder made from polytetrafluoroethene (PTFE) and two high density polyethylene (HDPE) caps that are used to screw on each end for easier access and removal of the sample. The seeded material makes ice from 200 g of distilled H_2O with 20 ppm of sodium dodecyl sulfate (SDS) and then crushed, ground, and sieved to 300 μm grain size and placed into the molds. The methane hydrate formation occurs during the pressurization, heating, cooling, and depressurization process with reaction vessel. At the end of the process, the pressure from the reaction vessel is quickly released in order to take out the methane hydrate sample and swiftly store them. Hydrate formation is monitored by a data

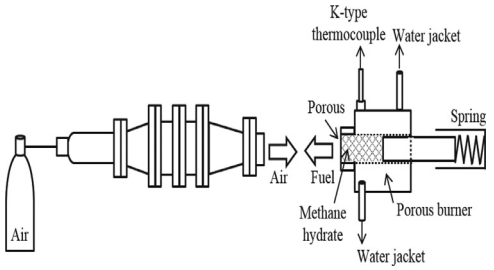

Fig. 1. The schematic diagram of an opposed-jet porous burner.

acquisition system to observe the P–T conditions through the entire heating and cooling process.

2.2. Development of the opposed-jet porous burner for methane hydrate combustion

The opposed jet burner, with its outstanding feature of a 1-D flat flame is a standard configuration [17] used for close comparison with theoretical and numerical analyses, has been extensively used for fundamental studies of various flame parameters and flame structures. Design modifications for the opposed jet burner [13] were implemented to accommodate the combustion challenges associated with methane hydrate fuel, such as the initial solid phase, the self-preservation problem, and the unsteady methane release. Fig. 1 shows the schematic of the opposed jet porous burner. The flame configuration represents a strained, laminar, one dimensional flat flame, and its dynamics are well considered and determined. Because of the one dimensional nature of the flow field, the fuel released by the hydrate diffuses and burns with the oxidizer. In the present study, the strain rate a, based on, V_F and V_O, fuel and air velocity, respectively, is set to a fixed value defined as [18]:

$$a = \frac{2V_O}{L}\left(1 + \frac{V_F}{V_O}\sqrt{\frac{\rho_F}{\rho_O}}\right) \quad (1)$$

where ρ is density. The gap, L, between the fuel side and the oxidizer side is 5 mm and the diameters of the fuel and oxidizer burner ducts are both 12 mm. The flow rate of the oxidizer is set to 700 SCCM and was measured using a Cole Parmer rotameter with an uncertainty of $\pm 0.2\%$ of full scale. The faces of the opposed-jet porous burner are aligned so that their centerlines are along the same axis. The fuel side of the porous burner contains the methane hydrate. A piston pushed by a spring is employed to exert an adjustable force on the hydrate. The applied force will constantly move the hydrate toward the interior porous wall of the burner; the water from the melted ice was drained in order to maintain a steady release of methane and to avoid the self-preservation problem. Therefore, the flow rate of fuel depends on the dissociation rate of the methane hydrate. The yellow region shown on the schematic is used for placing the hydrate. A circulating ethanediol bath is employed to maintain the temperature of the burner at approximately 280 K in order to avoid significant methane release during the loading process. The temperature inside the burner is monitored by a sheathed K-type thermocouple. The burner is ignited with a small torch, and a digital SLR camera is used to record the combustion process.

2.3. Thin filament pyrometry (TFP)

The study uses a technique that merges thin-filament and color-ratio pyrometry using a digital color camera to measure the hydrate flame temperature. The combination approach allows TFP to measure lower temperatures than when using color-ratios alone. The details on the calibration of the camera sensor are discussed in Llad'o et al. [19] and Ma et al. [20]. The spectral sensitivity of the cameras detector is obtained for all three channels (R,G,B) and through integrated radiation calculation a table that correlates color ratio of temperature is created. For the measurement a 15 μm fine SiC Ceramic Grade (CG) Nicalon fiber is positioned in the flame and the emission due to thermal radiation from the heated portion is captured using a Nikon D-80 camera. The RGB values are extracted from the image and then correlated to the gas temperature. TFP is known for its high spatial resolution (100 μm [21]), fast temporal response (1 ms) [22], and its convenience to get line measurements rather than at a point. All these characteristics make TFP a suitable method for measuring temperatures in unsteady and flickering flames like hydrates and in flames with high and variable temperatures that make radiation correction difficult. The SiC fiber is positioned inclined across the flame and the light radiating from the flame heated portion is captured by the Nikon D80 camera. The position of the SiC fiber in the vicinity of the burner and the flame are shown in Fig. 2. This is not an image shown for processing temperature; the images that are evaluated for temperature do not show the flame and have a shorter exposure time. The angle of the fiber is about 8° to make sure the fiber crosses the flame and gives a long region of heated fiber. The camera settings that provided the best color signatures were an ISO of 200, an aperture of f/6.3 and an exposure time of 1/80 s. The camera is integrated with a BG40 color filter (SCHOTT Inc.) which is used to balance the intensity in the three RGB channels.

2.4. Computational methods

Detailed chemistry computations were performed using the Opposed flow Flame Simulator of CHEMKIN PRO [23]. The GRI 3.0 mechanism, with its 325 elementary chemical reactions

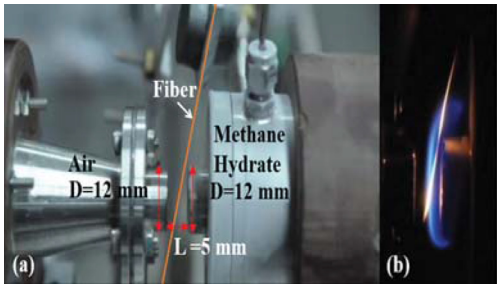

Fig. 2. (a) The schematic shows the position of the SiC fiber and burner (b) SiC fiber inclined across the methane hydrate flame.

and 53 species, was used [24]. The GRI mechanism was compared with another well-validated mechanism (Galway) [25] and no obvious differences were observed in flame temperature and flame extinction. In addition, most studies in the literature of steam dilution in methane flames use the GRI mechanism. The counterflow configuration is a standard configuration for kinetic modeling [17] and was used to idealize and simulate the hydrate combustion in a porous opposed jet burner. In this configuration the fuel stream is made up of fuel (methane) and water vapor injected from the fuel duct as part of the reactants, and an oxidizer stream of air is injected from the oxidizer duct. The fuel-side velocity and the strain rate remained constant with water addition. The distance between the fuel boundary and the oxidizer boundary is set to $L = 5$ mm. The flow field is characterized through the global strain rate as defined from Eq. 1 with velocity conditions 8.6 and 10.3 cm/s, respectively for fuel and air. The air velocity was based on the measured flow rate and assuming a top-hat profile. The fuel velocity was estimated based on the flow rate of the methane and water vapor that is assumed to be entrained on typical hydrate flames. The fuel and water vapor mixture (hydrate fuel side) is set to the temperature matching the vapor pressure of water injected with the fuel (358 K) while the oxidizer side is set to the ambient temperature. This study investigated the flame structure parameters (temperature, position, and width) and compared them with experimental results of TFP measurements.

3. Experimental results

3.1. Methane hydrate combustion using the opposed-jet porous burner

The burning process of methane hydrates using the opposed-jet porous burner is shown in Fig. 3. After ignition, the blue flame rapidly moves to become a flat flame between the two opposed circular jets and the flame burns steadily for more than 5 s. After this stable burning phase, the flame becomes twisted and unstable until it extinguishes. The unstable and twisted flame in the latter part of the process is due to the nonuniform methane release as an effect from the blockade of accumulated water at the porous head end. Nevertheless, the flat and stable flame period is sufficiently long to permit experimental flame diagnostics. These diagnostics are difficult to accomplish in free burning hydrates [13] because of unstable burning, water dripping, and self-preservation. The hydrate flame is blue in color, unlike the generic methane hydrate flame which can be orange in color due to soot inception [26]. Some have proposed that the soot reduction that appears on these flames occurs as a result of hydroxyl radicals that are present from the water addition, which leads to the enhanced oxidation of soot precursors such as acetylene [14]. The methane release rate as a function of the ambient pressure and temperature is an important parameter used for the modeling of methane hydrate combustion. Nevertheless, the database for the methane release rate from methane hydrate is not well established. Since the steady flame implies steady methane release, the opposed-jet porous burner can be used to measure the methane release rate from the methane hydrate. A digital electronic scale with high precision of 0.01 g monitors the transient variation in the total mass of the burner and hydrate during the burning process; a thermocouple is attached to the porous burner wall to monitor the temperature during the combustion process. The scale was used to measure the variation of the methane hydrate weight for every test case. For every experiment

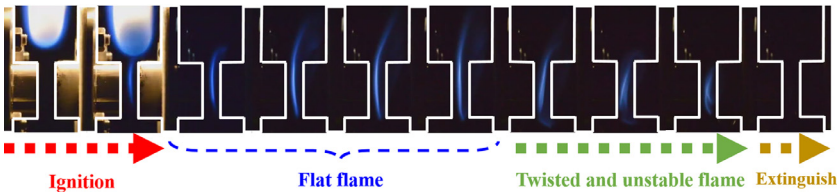

Fig. 3. The burning process of a methane hydrate flame in an opposed-jet porous burner.

the variation of methane hydrate weight was recorded for 300 s until no further weight change was observed. The data was correlated by a linear regression analysis; a straight line fit through the data provided a methane release rate gradient. The experiment was repeated 5 times which provided an average methane release rate of approximately 5.8 mg/s with an uncertainty of 1 mg/s.

At the end of the experiment, only a small amount of water remains in the burner, and the wall temperature was slightly lower than the boiling temperature of water. According to the previous work [13], the blue flame of the opposed-jet porous burner in Fig. 3 is thought to be due to combustion of methane gas laden with sufficient quantity of water vapor and perhaps tiny water droplets. Any droplets of water in the methane gas evaporate when the flame approaches the burner. This highly moisture laden methane flame is the outstanding characteristic of methane hydrate combustion.

3.2. Experimental temperatures using TFP

Fig. 2 shows the emission from the SiC filament tilted across the flame to get the axial temperature profile from a single TFP image. Fig. 4 shows the measured mean methane hydrate flame temperature of approximately 1690 K after radiation correction, which is relatively low compared to a pure methane/air diffusion flame. More than one photo was captured during the burning process so the flame movement (peak temperature position) is a relative capture of the flame moving toward the air side as the total velocity of the methane and water release increased (as seen in Fig. 5).

The flame movement is also responsible for the methane release, i.e., the flame moves further from the burner in search of the stoichiometric condition where the air/methane fuel mixture burns. This movement controls the heat flux from the flame to the hydrate sample and is responsible for providing the heat for dissociation, melting, and evaporation of the water. The temperature profile is measured in the core reaction zone and can be seen in Fig. 5 with a width of 0.7 mm and a maximum temperature of 1700 K. The TFP temperature width is broader than that from the computations due partially to sensitive dependency of the angle in the tilted fiber. There is, however, a clear thickening of the measured flame relative to an ideal counterflow flame. The thickness can be due to variations from the ideal 1-D nature of the experimental system or due to a buoyant contribution at the very low flow velocities of the experiment. Since the burner is oriented horizontally, there can be a gravitational influence from top to bottom of the flame. The flame temperature decreases with the presence of water vapor due to the cooling and dilution effects in the methane release from the hydrate. The overall gas temperature uncertainty was estimated to be 50 K. This considered radiation correction, deviations from the gray body assumption, and errors in the camera calibration.

4. Computational results

Fig. 6 shows the predicted temperature profile for a water laden methane/air nonpremixed counterflow flame compared with hydrate combustion in a porous opposed-jet burner, $a = 60\ s^{-1}$ ($V_F = 8.6$ cm/s and $V_O = 10.3$ cm/s). The boundary conditions at the fuel inlet and oxidizer inlets are defined as $T_F = 358$ K, $T_O = 296$ K, respectively. The fuel side temperature was selected after first finding the water fraction that produced a flame temperature matching the experimental value. That water fraction was then converted to a saturation

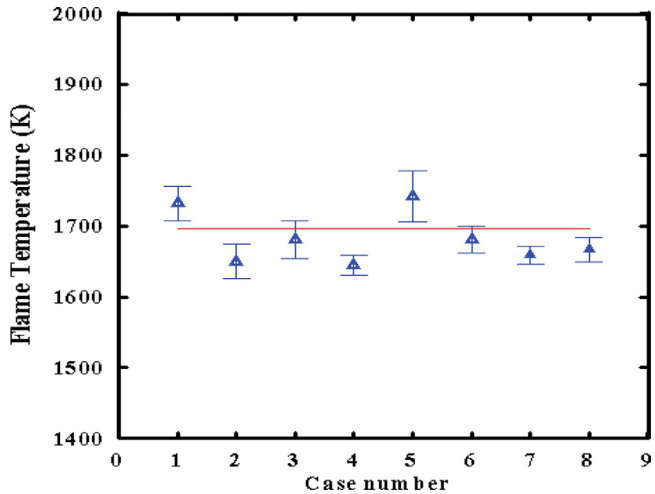

Fig. 4. The mean peak flame temperature of the opposed-jet porous burner by TFP measurement system.

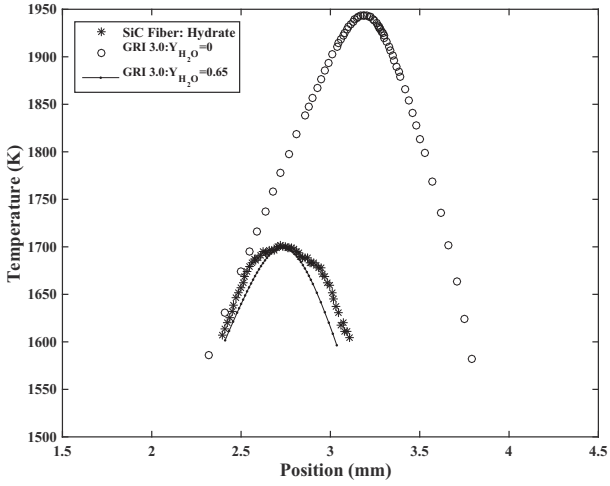

Fig. 5. Comparison of TFP and predicted temperature with no water added and near extinction, $Y_{H2O} = 0$ and $Y_{H2O} = 0.65$, respectively.

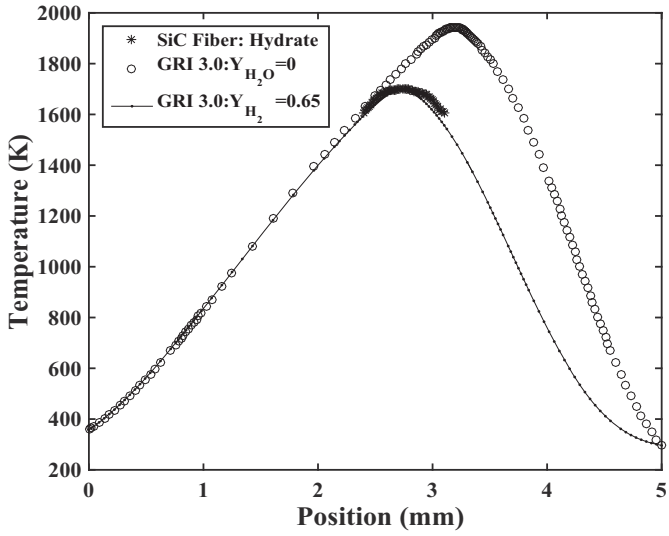

Fig. 6. Experimental TFP temperature measurements are compared to computational results: $a = 60\ s^{-1}$ with corresponding velocities for fuel and oxidizer, $V_F = 8.6$ cm/s and $V_o = 10.3$ cm/s, respectively.

temperature, which was used for the boundary condition. The temperature of the flame with varying water (Y_{H2O}) molar fractions is computed across a total gap distance of $L = 5$ mm, between the fuel at $L = 0$ mm and oxidizer burner at $L = 5$ mm. The peak flame temperature with no water added to a methane/air diffusion flame is 1944 K and positioned at 3.2 mm. The width of a flame with no water has a broader width (above 1 mm) than flames with an increase in the water mass fraction. The flame thickness decreases with water addition because the global strain rate increases with the water added to the fixed fuel flow rate. Higher strain rates produce thinner flames. The temperature is lower than adiabatic and this is because lower strain rate flames lose more heat to the fuel side burner. This is also apparent from the temperature gradient on both the fuel and oxidizer boundaries. The simulation was computed from 1:1 molar ratio of methane to water up to 1:1.7. There was no stable solution beyond 1.7 mol of water to 1 mole of methane.

The maximum peak temperature decreases as a function of an increase in the water mass fraction due to the water diluting the fuel and behaving as a thermal sink, shown in Fig. 7. The maximum temperature just prior to extinction of water laden methane flames is 1700 K with a mass water

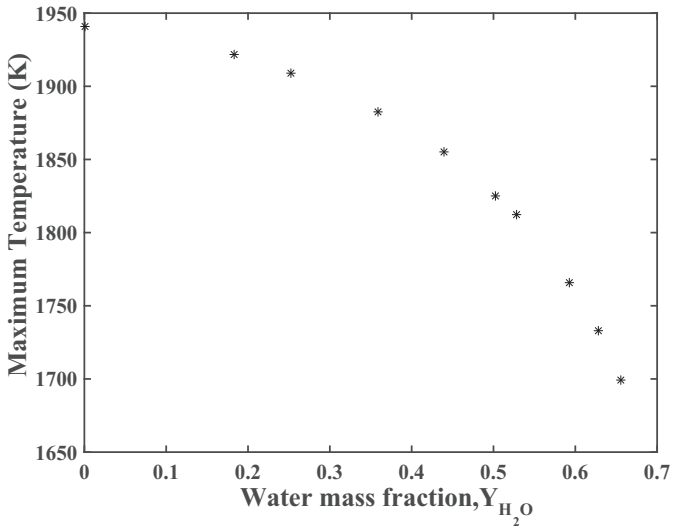

Fig. 7. Maximum temperature with mass fraction of water.

fraction of 0.65 and position of 2.7 mm. Flame movement is seen to agree between the experiment and computations showing the characteristic of the fuel and water vapor release during the combustion of a methane hydrate. Similar experimental temperatures at extinction are seen in Lee et al. [14] for extrapolated conditions equivalent to a water to methane molar ratio of 1.7 (mass fraction of 0.6); the peak extinction temperature corresponds to strain rates close to 164 s^{-1}. For these flames the decrease in temperature is due to a contribution from the increase in strain rate (i.e., total fuel side velocity), which included the contribution of water vapor. The predicted maximum amount of water that flames can sustain is comparable to the maximum amount of water vapor observed in the combustion of methane hydrates [27,28], indicating that the present flame configuration and chemical mechanism can provide thermal and chemical insight that occurs in hydrate combustion. One example is the discussion in the literature about whether addition of water leads to changes in the concentrations of important species that may lead to flame extinction, particularly the chain-branching radicals OH, H, and O. Lee et al. [14] reports the role of water as being primarily responsible in lowering the flame temperature and dilution whereas other studies report an increase in OH [13,29,30] and reduction of O, and H as evidence of a chemical effect. This discrepancy indicates that the role of water in flame extinction depends on the operating combustion conditions, such as the amount of fuel and air (equivalence ratio), flame temperature, the counterbalance of OH increase from depletion of O and H. With the accurate chemical model demonstrated it will be possible to explore the role of water in hydrate flame extinction.

5. Conclusions

In this study, we have shown that methane hydrate flames in porous burners can provide a steady and one dimensional flame that allow us to examine the mechanisms of heat and mass transfer that are key in the methane hydrate release. The feasibility of having a steady burning flame has facilitated temperature measurements using color ratio TFP with a calibrated Nikon D80 camera. The predicted and measured temperature, flame position, and flame width exhibit encouraging agreement using and indicate that the counterflow flame configuration provides insight into the thermal and chemical processes in the combustion of methane hydrates.

Methane hydrates flame temperatures in the opposed-jet porous burner are found to be approximately 1700 K, which corresponds to water to methane molar ratio of up to 1.7 (mass fraction of 0.6). The predicted maximum amount of water that flames can sustain is comparable to the maximum amount of water vapor observed in the natural combustion of methane hydrates, indicating that the opposed porous burner and counterflow configurations capture into the thermal and chemical processes that occur in humidified flames.

Acknowledgments

This research was partially supported by the National Science Council of Republic of China under Grant numbers NSC 101-2221-E-006-067-MY3. In addition, the W.M. Keck Foundation as part of the UCI Deep Ocean Power Science Laboratory.

References

[1] Y.F. Makogon, *J. Nat. Gas Sci. Eng.* 2 (2010) 49–59. http://www.sciencedirect.com/science/article/pii/S1875510009000754, doi:10.1016/j.jngse.2009.12.004.

[2] T. Yoshioka, Y. Yamamoto, T. Yokomori, R. Ohmura, T. Ueda, *Exp. Fluids* 56 (2015) 192. http://link.springer.com/10.1007/s00348-015-2041-4, doi:10.1007/s00348-015-2041-4.

[3] V. Yakushev, V. Istomin, Phys. Chem. Ice, Hokkaido University Press, Sapporo, 1992, pp. 136–139.

[4] S.Y. Misyura, V. Nakoryakov, *Energy & Fuels* 27 (2013) 7089–7097.

[5] G. Rehder, R. Eckl, M. Elfgen, A. Falenty, R. Hamann, N. Kähler, W.F. Kuhs, H. Osterkamp, C. Windmeier, *Energies* 5 (2012) 2499–2523. http://www.mdpi.com/1996-1073/5/7/2499/, doi:10.3390/en5072499.

[6] V.E. Nakoryakov, S.Y. Misyura, S.L. Elistratov, A.Y. Manakov, A.E. Shubnikov, J. Eng. Thermophys. 22 (230) (2013) 87–92, doi:10.1134/S181023281302001X.

[7] L.A. Stern, S. Circone, S.H. Kirby, W.B. Durham, *J. Phys. Chem. B* 105 (2001) 1756–1762 http://pubs.acs.org/doi/abs/10.1021/jp003061s$\delimiter"026E30F$nhttp://pubs.acs.org/doi/pdfplus/10.1021/jp003061s, doi:10.1021/jp003061s.

[8] T. Bar-Kohany, W.A. Sirignano, *Combust. Flame* 163 (2016) 284–300.

[9] Y. Maruyama, M.J. Fuse, T. Yokomori, R. Ohmura, S. Watanabe, T. Iwasaki, W. Iwabuchi, T. Ueda, *Proc. Combust. Inst.* 34 (2013) 2131–2138. http://www.sciencedirect.com/science/article/pii/S1540748912002878, doi:10.1016/j.proci.2012.06.179.

[10] Y. Nakamura, R. Katsuki, T. Yokomori, R. Ohmura, M. Takahashi, T. Iwasaki, K. Uchida, T. Ueda, *Energy & Fuels* 23 (2009) 1445–1449.

[11] K. Kitamura, K. Nakajo, T. Ueda, in: Proceedings of the Fourth International Conference on Gas Hydrate, pp.1055–1058.

[12] P. Taborek, D. Dunn-Rankin, W.M. Keck Foundation- Grant Abstracts 2013, 2012. http://www.wmkeck.org/grant-programs/research/medical-research-grant-abstracts/science-and-engineering-2012.

[13] F.-H. Wu, Y.-C. Chao, *Combust. Sci. Technol.* 2 (2015) 1–15.

[14] S. Lee, R. Padilla, D. Dunn-Rankin, T. Pham, O.C. Kwon, *Energy* 93 (2015) 442–450. http://www.sciencedirect.com/science/article/pii/S0360544215012578, doi:10.1016/j.energy.2015.09.047.

[15] I. Stern, S. Kirky, W.B. Durham, *Sci. -AAAS-Week. Paper Ed.* 273 (1996) 1843–1847.

[16] A. Biasioli, *Methane hydrate growth and morphology with implications for combustion, Master's thesis*, Politecnico di Milano, 2015.

[17] H. Tsuji, *Prog. Energy Combust. Sci.* 8 (1982) 93–119. http://www.sciencedirect.com/science/article/pii/0360128582900156, doi:10.1016/0360-1285(82)90015-6.

[18] K. Seshadri, F.A. Williams, Int. J. Heat Mass Transfer 21 (1978) 251–253.

[19] A. Llad'o, R.E. Padilla, D. Dunn-Rankin, T.K. Pham, in: 9th U.S National Combustion Meeting, CINCINNATI, OHIO, 2015, pp. 1–11.

[20] B. Ma, G. Wang, G. Magnotti, R.S. Barlow, M.B. Long, *Combust. Flame* 161 (2014) 908–916. http://www.sciencedirect.com/science/article/pii/S001021801300388X.

[21] W. Pitts, *Pro. Combust. Inst.* 29 (1996) 1171–1179.

[22] L.P. Goss, V. Vilimpoc, B. Sarka, W.F. Lynn, *J. Eng. Gas Turbines Power* 111 (1989) 46, doi:10.1115/1.3240226.

[23] R.J. Kee, J.A. Miller, G.H. Evans, G. Dixon-Lewis, *Symp. (Int.) Combust.* 22 (1989) 1479–1494. http://www.sciencedirect.com/science/article/pii/S0082078489801584, doi:10.1016/S0082-0784(89)80158-4.

[24] G.P. Smith, D.M. Golden, M. Frenklach, N.W. Moriarty, B. Eiteneer, M. Goldenberg, C.T. Bowman, R.K. Hanson, S. Song, W.J. Gardiner, et al., in: Gas Research Institute, Chicago, IL, 2000.

[25] E.L. Petersen, D.M. Kalitan, S. Simmons, G. Bourque, H.J. Curran, J.M. Simmie, *Proc. Combust. Inst.* 31 (2007) 447–454 270.

[26] C. Zhang, A. Atreya, K. Lee, *Symp. (Int.) Combust.* 24 (1992) 1049–1057. http://www.sciencedirect.com/science/article/pii/S0082078406801244, doi:10.1016/S0082-0784(06)80124-4.

[27] M. Roshandell, *Combustion of Methane Hydrate, Ph.D. thesis*, University of California, Irvine, 2013.

[28] J.S. Santacana Valle, D. Dunn-Rankin, in: 25th ICDERS, Leeds, UK, pp. 1–6.

[29] A. Mazas, B. Fiorina, D. Lacoste, T. Schuller, *Combust. Flame* 158 (2011) 2428–2440. http://www.sciencedirect.com/science/article/pii/S001021801100160X, doi:10.1016/j.combustflame.2011.05.014.

[30] J.S. Atreya A., in: International Conference on Fire Research and Engineering, Orlando, FL, September 10-15, 1995, pp. 103–108.